

Mechanism of the intermittent motion of two-phase debris flows

Liqun Lyu¹ · Zhaoyin Wang¹  · P. Cui²

Received: 12 November 2015 / Accepted: 7 September 2016 / Published online: 20 September 2016
© The Author(s) 2016. This article is published with open access at Springerlink.com

Abstract A typical two-phase debris flow exhibits a high and steep flow head consisting of rolling boulders and cobbles with intermittent or fluctuating velocity. The relative motion between the solid phase and the liquid phase is obvious. The motion of a two-phase debris flow depends not only on the rheological properties of the flow, but also on the energy transmission between the solid and liquid phases. Several models have been developed to study two-phase debris flows. An essential shortcoming of most of these models is the omission of the interaction between the two phases and identification of the different roles of the different materials in two-phase debris flows. The tracer particles were used for the velocity of solid phase and the velocity of liquid phase was calculated by the water velocity on the surface of the debris flow in the experiments. This paper analyzed the intermittent feature of two-phase debris flows based on videos of debris flows in the field and flume experiments. The experiments showed that the height of the head of the two-phase debris flow increased gradually in the initiation stage and reached equilibrium at a certain distance from the start of the debris flow. The height growth and the velocity of the flow head showed fluctuating characteristics. Model equations were established and the analyses proved that the average velocity of the two-phase debris flow head was proportional to the flood discharge and inversely proportional to the volume of the debris flow head.

Keywords Two-phase debris flow · Intermittent motion · Unsteady flow · Flow power · Energy dissipation

✉ Zhaoyin Wang
zywang@tsinghua.edu.cn

¹ State Key Laboratory of Hydrosience and Engineering, Tsinghua University, Beijing, People's Republic of China

² Mountain Hazard and the Earth's Surface Processes Key Laboratory, Institute of Mountain Hazards and Environment, Chinese Academy of Sciences, Chengdu, People's Republic of China

1 Introduction

Debris flows are widely distributed and frequently occurring hazard in mountainous regions. Chinese people call this phenomenon “dragon” because of its powerful and irresistible nature [1, 2]. Many different types of mass movements are regarded as debris flows [3]: debris torrents, debris floods, mudflows, mudslides, and hyperconcentrated flows. It is more important to classify debris flows according to their dynamic characteristics. The forces that support the largest particles during the movement of these kinds of flows mainly result from two actions [4]: the dispersive pressure resulting from collisions among the particles [5] and the plastic strength of the interstitial fluid when this is composed of a clay or mud slurry [6]. Turbulence of the interstitial fluid generally is too weak to support the largest particles [7]. For each specific type of flow, different rheological schemes using one of the two cited mechanisms are generally applied [8].

Based on the composition of the solid materials and fluid, debris flows are also classified as one-phase debris flows and two-phase debris flows [9]. One-phase debris flow is non-Newtonian, has a large yield stress, and exhibits laminar flow and intermittent features in many cases. In two-phase debris flows, the solid phase consists of gravel and boulders and the liquid phase consists of water with clay and silt in suspension [10]. The relative motion between the solid phase and the liquid phase is obvious [9].

Pudasaini [11] presented a comprehensive and real two-phase debris mass flow model that includes many of the essential physical phenomena of particle fluid mixture flows with strong interactions between the phases. It applies the Mohr–Coulomb plasticity for the solid stress, and the fluid extra stress is modeled as a non-Newtonian viscous stress that is enhanced by the solid volume fraction gradient. The generalized interfacial momentum transfer is modeled by including the force on the particle phase due to viscous drag, buoyancy, and the relative acceleration between the solid particles and the fluid (the virtual mass). The generalized drag force covers both the solid-like and fluid-like contributions in the mixture. The model has been applied to different types of subaerial and submarine mass flows including submarine landslides [12, 13], two-phase rock-ice avalanches with dynamic strength weakening and interphase mass and momentum exchanges [14], and in simulating a real two-phase glacial lake outburst flood [15]. In this work, debris flows are defined as flows that composed of mixtures of water and non-cohesive and relatively large particles, which corresponds to stony debris flows. For this kind of debris flow, a two-phase approach is of fundamental importance, because the stoppage of the debris flow is mainly induced by sedimentation of the coarser fraction and consequent separation of the water. Visco-plastic debris flows or mudflows are not discussed in this paper, in which the stoppage is the result of reduction of stresses below a threshold value [15, 16]. Hence, a one-phase debris flow denotes a muddy-debris flow, while a two-phase debris flow denotes a stony debris flow in this research.

Debris flows can be analyzed by applying different constitutive equations. Johnson and Rohm [17] and Yano and Daido [18] both postulated that debris flow material behaves as a single-phase homogeneous visco-plastic continuum. Several researchers have applied their models to study one-phase debris flows [19, 20]. A one-phase debris flow can develop from a continuous flow into an intermittent flow composed of a series of roll waves [21]. Because there is no collision between particles, and, thus, little internal energy dissipation; the velocity of a one-phase debris flow is very high in steep gradient gullies, even higher than the velocity of the water flow [22]. One-phase debris flows in the Jiangjia Ravine in southern China often develop into intermittent flows with velocities exceeding 15 m s^{-1}

[23]. The high velocity was measured with a double radar velocimeter, which receives high frequency radio waves reflected from the head of the debris flows. The highest velocity was measured at 26.8 m s^{-1} [24]. However, the one-phase debris flow as a single-phase homogeneous visco-plastic continuum was predicted to have a flow velocity much lower than the water flow because the viscosity and yield shear stress of the debris mixture is much greater than that of the water. In fact, the velocity of one-phase debris flows in the Jiangjia Ravine in southern China is often two times higher than that of the flood flows in the same gully [22]. Because the clay and silt particles in the debris mixture exhibit a “paving the way process” resulting in a smooth rough bed, they produce a residual layer, on which debris flow surges move at a high velocity. The ratio of drag reduction of the movable-bed, R , can be as high as 60 %, $R = (n_w - n_d)/n_w$, where n_w and n_d are the Manning’s roughness coefficient for water flows and debris flows, respectively [25].

Debris flows in mountain torrents of the Austrian, Italian, Swiss Alps and Sichuan and Tibet in southwest China primarily are two-phase debris flows [9, 26], because the solid materials in these areas consist of many boulders, cobbles, and gravel [27–30]. Sand, silt, and clay make up only a small portion of the loose solid materials in these areas. In two-phase debris flows, cobbles and boulders collide with each other and consume most of the flow energy. The velocity of two-phase debris flows is much lower than that of one-phase debris flows [10]. A typical two-phase debris flow exhibits a high and steep head consisting of rolling boulders and cobbles with an intermittent or fluctuating velocity. The mean-velocity of a two-phase debris flow depends on the river slope and the water content. The velocity of a two-phase debris flow was measured by the authors at $0.5\text{--}1.5 \text{ m s}^{-1}$ in the Yinchang Ravine located in southwest China in 2011.

Bagnold [31] made the most prominent early efforts to construct a model that accounts for particle collisions. The core of this model is the concept of dispersive force. The model postulates that the debris is a mixture of a dilatant fluid but the shear stress is generated mainly by collisions between particles, $\tau \propto (\lambda D)^2 (du/dy)^2$. Many researchers have applied this model to study two-phase debris flows [32–34]. Constitutive equations can be applied only if all parts of the flow behave the same way rheologically and these equations can be used only for neutrally buoyant flows, which is not true for most debris flows [11]. The recent general two-phase debris flow model proposed by Pudasaini [11] overcomes this deficiency by including the strong interactions between the solid particles and viscous fluid with different rheological models for solid and liquid phases [13, 35]. The energy transmission from the flowing water to particles and then to the debris flow head plays a key role for the debris flow. In summary, two-phase debris flows are more complex than one-phase debris flows and the motion of a two-phase debris flow depends not only on the rheological properties of the flow, but, more importantly, on the energy transmission between the solid and liquid phases [11]. Therefore the flow is hard to analyze by applying a single-phase constitutive equation and the energy transmission from water to sediment particles and the head of the debris flow is an important aspect to study.

Field data on debris flows are of utmost importance for improving knowledge on the complicated movement of debris flows. For example, a pair of ultrasonic, seismic, or acoustic sensors placed at a known distance from each other along a torrent offers a method to obtain the mean front velocity of debris flows [36]. An observation system developed in the Acquabona channel provides information on the initiation, dynamics, and deposition of debris flow [37]. Video cameras, ultrasonic devices, a radar device, geophones, and rain gauges equipped in three Swiss debris flow prone watersheds have provided essential information towards improving the understanding of the mechanisms of debris flow [38]. Other important debris flow variables, namely, the peak discharge and flow volume, were

estimated from instrumental records [39]. However, the sudden and often unpredictable occurrence of debris flows makes it very difficult for observers to be present at the moment of debris flow occurrence and use these methods to monitor the debris flows.

Many scientists have studied debris flows by flume experiments. The fluid dynamics of stony debris flows generated in two small tributaries adjacent to each other and flowing into a main receiving channel was analyzed experimentally at a laboratory scale [40]. The unit critical discharge to generate a mature, uniform debris flow with uniform debris material was analyzed in a laboratory flume with a slope angle between 16° and 19° [41]. Wang and Zhang [42] studied the initiation of two-phase debris flows experimentally in a 10 m-long and 50 cm-wide tilting flume with glass-sided walls.

The initiation of a debris flow is often a consequence of intensive bed erosion and bank erosion resulting from water flow [43–48]. The motion of debris flows depends on the incoming discharge of the water flow [49]. Boulders and cobbles play an important role in the formation of the debris flow head [50–52]. Generally, the head grows at the beginning of the debris flow development and then reaches an equilibrium height [21, 53]. It was observed that the water content in the head was low, and sometimes only dry particles moved in the very front of the head [54]. The velocity of the liquid phase and the particles in the following part of the head was higher than the moving speed of the head.

Many experimental studies were done with rectangular cross-sectional flumes and the effects of gully bank erosion and bank collapse were not simulated [55–57]. Experiments in this study were conducted using a trapezoidal cross-section gully model to simulate gully bank erosion and bed erosion. The motion of the debris flow head was intermittent or fluctuating, which was mainly caused by the imbalance between the energy dissipation and energy supply from the flowing water. The energy transmission between the two phases is discussed and formulated in the following sections.

2 Research methods

The intermittent motion of two-phase debris flows was analyzed based on videos of field debris flows and flume experiments. After the 2008 Wenchuan earthquake in China, massive landslides and collapses occurred on the banks of mountainous gullies in Sichuan province in southwest China. The loose, coarse particle materials from these landslides and collapses were easily moved by floods caused by rainstorms into the gullies and formed debris flows. A massive debris flow occurred in the Yinchang Gully (coordinates of the gully toe: $103^\circ47'03''\text{E}$, $30^\circ43'45''\text{N}$) in Sichuan province in 2011 and a valuable video of the debris flow passing through a highway was recorded. After the 1950 Chayu earthquake in China, frequent debris flows have occurred in the Guxiang Gully (coordinates of the gully toe: $95^\circ27'21''\text{E}$, $29^\circ53'23''\text{N}$) in Tibet. A heavy debris flow, which occurred in 1964 at this location, was recorded. By comparing the objects in the videos, the changing of the height and velocity of the two recorded debris flows with time were determined. It was found that both debris flow events had obvious intermittent features. Figure 1a shows the sediment size distributions of the upper, middle, and lower reaches of the Guxiang Gully and the middle and lower reaches of the Yinchang Gully. The clay content of these two gullies was significantly lower than that of the Jiangjia Gully in Yunnan province located in southwest China, which is prone to one-phase debris flows [58, 59]. More than 80 % of the particles in these two gullies had diameters ranging between 0.5 and 1 m, which is typical for two-phase debris flows.

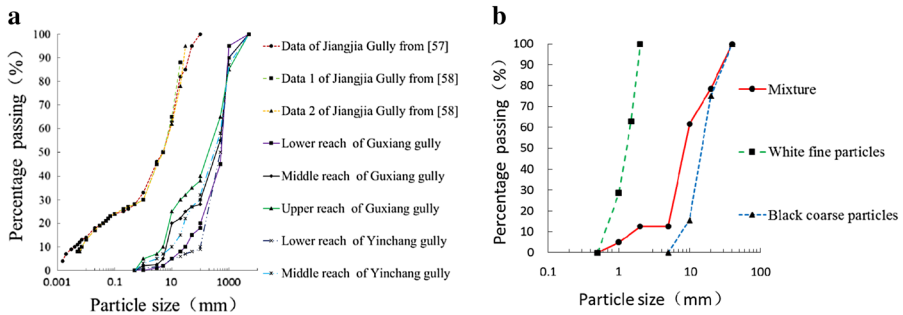


Fig. 1 Sediment size distributions for natural and experimental debris flows. **a** Sediment size distributions of natural debris flows, **b** sediment size distributions of the experiments

The intermittent motion of two-phase debris flows in nature was simulated via flume experiments. Experiments were carried out in a laboratory flume installed in the Institute of Mountain Hazards and Environment, Chinese Academy of Sciences. A 12 m-long and 0.6 m-wide flume was tilted by a telescopic piston to a slope angle of 18° (Fig. 2a). There was a water tank (3.94 m long \times 1.25 m wide \times 0.98 m high) at the upper end of the flume, and the water was released through a small hole at the bottom of the water tank. Preliminary experimental results are summarized in Table 1, which are discussed in Sect. 3. The water level in the tank was kept constant, so the water discharge from the hole

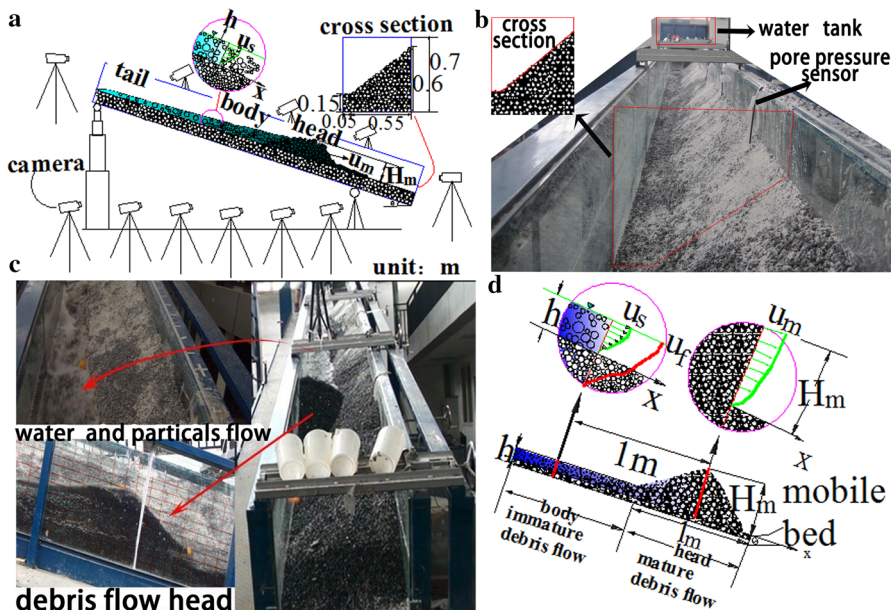


Fig. 2 Experimental flume. **a** Side sketch of the flume, **b** front view of the flume, **c** debris flow head and body, **d** velocity distributions of the head, particles, and water flow at the body

Table 1 Experimental results

Experimental properties	1	2	3	4	5	6
Water discharge, Q (L s^{-1})	6.720	13.380	20.250	25.650	33.620	36.210
Average height of debris flow head at 7–9.5 m, $\overline{H_m}$ (m)	0.445	0.375	0.367	0.328	0.360	0.352
Average length of debris flow head at 7–9.5 m, $\overline{l_m}$ (m)	2.510	1.690	1.120	1.090	1.060	0.910
Run duration, T (s)	79	43	28	24	18	15
Average velocity of debris flow head, $\overline{u_m}$ (m s^{-1})	0.120	0.220	0.340	0.400	0.530	0.680
Number of interim periods	10	4	2	3	3	2
Average velocity of water, $\overline{u_f}$ (m s^{-1})	0.440	0.540	0.770	0.850	1.040	1.180
Average velocity of particles, $\overline{u_s}$ (m s^{-1})	0.240	0.310	0.500	0.550	0.720	0.820
Average height of flow layer behind the flow head, \overline{h} (m)	0.050	0.070	0.075	0.080	0.090	0.100
Sediment volume content of the flow head, c_g (%)	61.3	60.1	60.8	61.9	60.0	60.1
Water volume content of the flow head, c_w (%)	1.2	2.1	2.6	3.0	3.2	3.5
Sediment volume content behind the flow head, c_g (%)	52.8	51.7	51.6	50.8	49.7	46.0
Water volume content behind the flow head, c_w (%)	47.2	48.3	48.4	49.2	50.3	54.0

was constant. The water discharge could be controlled by changing the opening size of the hole. In order to keep the water level constant in the tank, water needed to be injected continuously into the tank by a pump, and the water injection led to slight fluctuations of the water level in the tank. Therefore, the water discharge in Table 1 is not strictly constant. For each opening size of the hole, the water discharge was obtained by collecting water at the outlet of the hole and then calculating the discharge. The highest deviation of each repeated discharge measurement from the averaged water flow discharge parameters in Table 1 was 3 %. The 12-m-long flume was divided into two sections: an upper section and a lower section. The upper 2-m-long section was the fixed bed section for stabilizing the jet flow released from the hole at the bottom of the tank. The lower 10-m-long section was the movable bed section and the water would scour the movable bed section and produce the debris flow. The sediments were not stable at the end of the flume if no stopper was placed at the outlet. Seepage flow was made possible by using a permeable sill located at the end of the flume, which sustained the loose sediment bed despite the slope, while allowing ground water flow. An automatic collection device was placed at the flume outlet for collecting water and sediments and measuring the concentrations of water and sediment in different parts of the debris flow. The flume was 0.6 m wide, 0.55 m of which was the bank (Fig. 2b).

Due to lateral erosion and high roughness of the erodible banks, the frictional resistance near the gully bank is higher than that within the bottom of the debris flow body. Therefore, the transverse distribution of the longitudinal velocity is usually that the velocity along the longitudinal center line in the cross section is higher than the velocity across the lateral line. Lateral erosion processes affect the velocity distribution in two different ways: first, the additional mass falling into the flow causes an increase in the bed friction force per unit mass; and second, the additional mass generates a resistive force on the moving mass

because of the momentum transfer between the debris flow in motion and the particles from the bank that have to be mobilized and accelerated to match the flow velocity [60]. The approach proposed in this paper does not allow the particles' longitudinal velocity to be described. However, the particles' velocity distribution along the longitudinal centerline is necessary for the analyses of the intermittent motion. The frictional resistance near both banks of a gully in nature was assumed to be the same. This boundary condition made the calculation domain axisymmetric, and, hence, calculations were performed on only half of the profile. The experimental measurements were interpreted as if the glass sidewalls, often with smooth surfaces, did not play a major role in the flow dynamics relative to the erosional bank. The flow resistance near the glass sidewalls was lower than the flow resistance near the gully bank, and thus, the distribution of the longitudinal velocity near the glass sidewalls could represent the particles velocity along the longitudinal centerline. Of course, a number of limitations related to this geometry may influence the debris flow features. However, it is believed that this approach is appropriate for the analyses of debris flow motion.

The experimental sediment was a mixture composed of coarse and fine particles with different colors: black coarse particles (5–40 mm) and white fine particles (0.5–2 mm). The sediments were natural particles from a debris flow fan of the Yinchang Gully previously mentioned above, which was only 90 km from the laboratory of the Institute of Mountain Hazards and Environment. The particle–fluid density ratio was $\rho_s/\rho_w = 2.65$. Compared with the natural debris flow sediments, the experimental sediments did not contain particles with diameters above 50 mm. The size distributions of the experimental sediments are shown in Fig. 1b. The volume concentration of the experimental sediments, c_v , was 0.65. In all experiments, the flow was seeded with a small proportion of white tracer particles (1 % by weight). The d_{50} was 5–40 mm for the black coarse particles size, 0.5–2 mm for the white fine particles, and 5–10 mm for the white tracer particles. The white tracer particles were used for easier visual observations, and could be manually tracked on video images to provide a preliminary idea of the mean velocity profile across the depth of the debris flow at given cross sections. Transparent glass was used for the channel walls, and debris flows were photographed through the transparent flume sidewall using a total of 11 cameras: 6 at the side, 3 at the front, 1 at the upper reach, and 1 at the lower reach (Fig. 2a). Because of the high sediment concentration of the debris flow, the water velocity at the middle and lower layers of the debris flow was hard to be measure, and only water velocity on the surface of the debris flow was measured.

3 Experimental results

A total of six experiments were carried out for this study. In all of the experiments, there were always debris surges at the front of the debris flow, which were higher than the debris flow body, as shown in Fig. 2a, c. The higher debris surge at the front is called the debris flow head [14]. As shown in Fig. 2c, d, a debris flow can be separated into the head part and the body part. The water content of the head is low and there is no water flow on the surface of the head, which is a mature debris flow; the water content of the body is high and there is water flow on the surface of the body, which is an immature debris flow [60, 61]. The velocity distributions of the head, particles, and water flow at the body are shown in Fig. 2d. The height of the debris flow head, H_m , refers to the vertical distance from the highest point of the debris surge to the movable bed surface. The velocity of the debris flow

head, \overline{u}_m , refers to the depth-averaged velocity of the particles flow at the cross section from the highest point of the debris surge to the movable bed surface. The height of the body flow layer behind the flow head, h , refers to the vertical depth of the moving cross section, which was always 1 m behind the highest point of the debris flow head. The velocities of the water flow, \overline{u}_f , and particles flow, \overline{u}_s , of the body refer to the depth-averaged velocities of the water flow and the particles flow at the cross section, which was always 1 m behind the highest point of the debris flow head. Not all the values of \overline{u}_f and \overline{u}_s at every flume cross section are reported in this paper because the purpose of this paper is to discuss the depth-averaged velocity of the body section near the debris flow head. And the body section was the section which was always 1 m behind the highest point of the debris flow head. The preliminary experimental results are listed in Table 1. The velocities of the water and particles were obtained based on images taken by the 11 cameras. The videos were converted into still images at a rate of 25 frames per second. The displacement and velocity of the tracer particles were calculated based on the individual images. The average velocity of the particles flow was calculated by averaging the velocities of the particles at different depths of the flow layer. The velocity of the water was assumed to be one half of the water velocity on the surface of the flow, although this assumption was not accurate.

Sampling and measuring the water content of the head and body of the debris flow in the flume may disturb the movement and video process. However, sampling the head and body of the debris flow when each part reached the outlet of the flume and measuring the water content was easier. Although the water content of the head and body at the outlet of the flume was different from the water content of the head and body at the different sections of the flume, the phenomenon that the water content of the head was much lower than the water content of the body at different sections of the flume was consistent. The length of the body was much longer than that of the head, hence, more than five mixture samples were taken when the body flowed out of the outlet. By contrast, only one mixture sample was taken when the head reached the outlet. The samples were dried to determine the masses of the sediment and water. The volume content of the sediment and water was calculated based on the masses and densities of the sediment and water. The content of the sediment and water of the body was the mean value from the 5 samples. The content of the sediment and water of the head was the value from the only one sample. The results showed that the water content of the body was higher than that of the head (Table 1). Since the flow head was highly unsaturated, the sum of the water and sediment volume concentration was less than 1.

The water released from the tank moved the sediments on the gully bed and banks, and along with the effects from bank collapse and bottom erosion, debris flow developed. At the initial stage of the debris flow formation, the particle concentration was low and the velocity of the flow head was fast. As the particle concentration and resistance of the flow head increased, the velocity of the flow head reduced then the motion of the flow head became intermittent. The debris flow consisted of only one head followed by a declining continuous body flow. The debris flow head moved discontinuously with static periods of zero flow rate, separating the passage of waves (relative to the body height) of a heavily debris-laden head. The debris flow head moved higher during the periods when the flow head moved downstream. The head waves were separated into intervals of zero velocity, which were called “the interim periods”, and intervals of higher velocity, which were called “the moving periods”, respectively. During the interim period, the flow head stopped moving, however, the water behind the flow head continued to carry particles to

the head. The particles, especially coarse particles, climbed onto the flow head under the effect of inertia. As a result, the flow head continued to become bigger and the pressure potential energy [62] continued to increase. When the pressure potential energy of the debris flow head became large enough, the flow head started to move downstream again under the action of gravity. During the moving period, the flow head height decreased and velocity increased. During the process of intermittent motion, the growth of the flow head fluctuated. The flow head height increased quickly during the early stage of the formation of the debris flow and then became relatively stable in the section from 7 to 9.5 m of the flume. Table 1 lists the average height and length of the debris flow head at distance 7–9.5 m, the motion time, the average velocity, and the number of interim periods when the flow head was passing through the entire flume. Figure 3 shows the typical fluctuating growth process of the debris flow head of experiments No. 1, 3, and 5. Results of experiment No. 1 showed that the head height during the moving periods (2, 10, 46, 64 s) was always lower than the peak height of the flow head during the interim periods (8, 39, 79 s) in every intermittent cycle, but the peak height of the debris flow head along the flume always first increased and then became relatively stable.

Figure 4 shows the growth process of the height of the debris flow head for different water discharges. Results of all six experiments showed that the height of the flow head increased when the flow head moved along the flume from 0 to 5 m and the peak height of the fluctuating wave tended to be stabilized from 7 to 9.5 m, and the lower the water discharge was, the more obvious the height fluctuation was.

Figure 5 shows the velocity of the debris flow head, and the average velocity of the water and particles flow behind the head. During the initial stage of the debris flow motion, the velocity of the flow head and the average velocity of the water and particles behind the head were faster. With the increase of the sediment content and energy consumption due to collisions and friction between the particles, the high flow head velocity decreased to zero

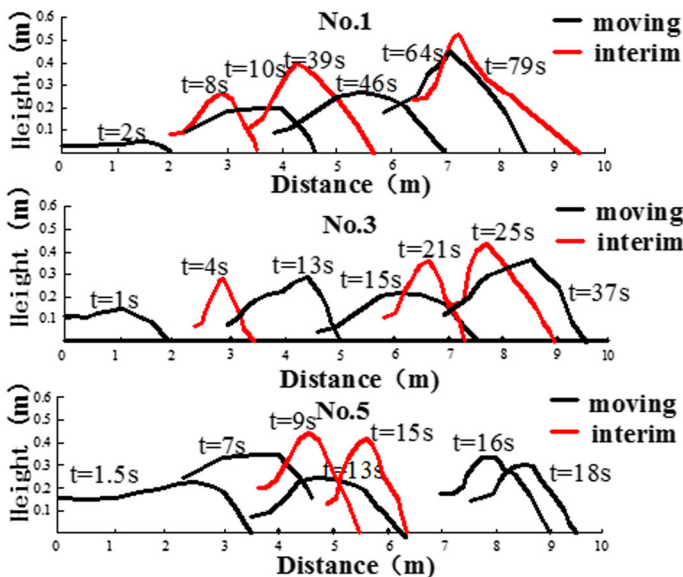


Fig. 3 Flow head height along flume

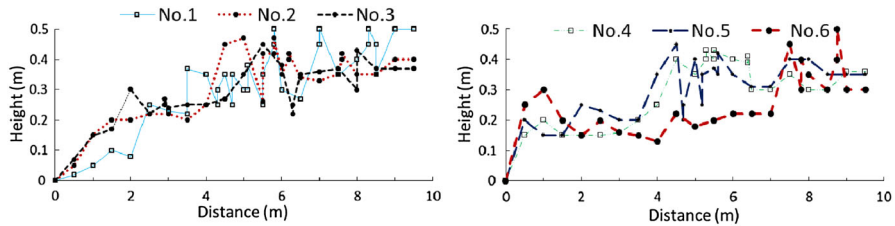


Fig. 4 Flow head height for different water discharges

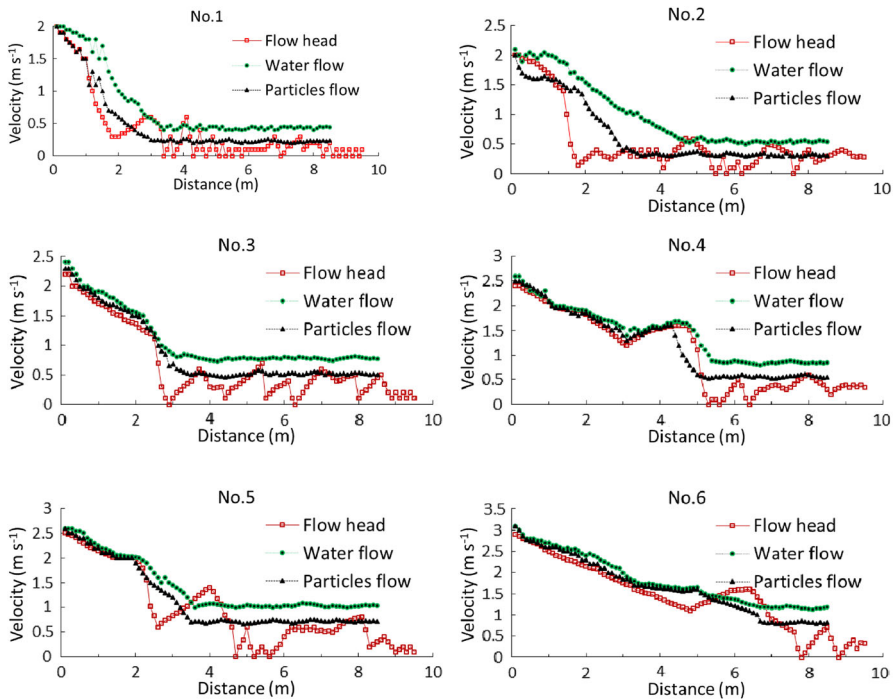


Fig. 5 Velocity of the flow head compared to the average velocities of the water and particles flow behind the flow head

and began to move intermittently. The average velocity of the water flow and particles flow behind the head tended to be stable during the process of intermittent motion of the flow head. Under different flow discharge conditions, the average velocity of the water flow was faster than that of the particles flow, which were both faster than the velocity of the debris flow head.

Figure 6a shows the velocity and height of two natural two-phase debris flows head, located in the Yinchang Gully and the Guxiang Gully, compared with the velocity and height of the two-phase debris flow head between 4 to 6 m of the flume in experiment No. 1 as shown in Fig. 6b. Figure 7 shows the shape of the debris flow head in the Yinchang Gully and that of the experimental debris flow. Due to the energy consumption at the flow head, the potential energy of the flow head could not support motion, and the flow head had to stop and wait for the energy supply from the water and particles behind. Particles

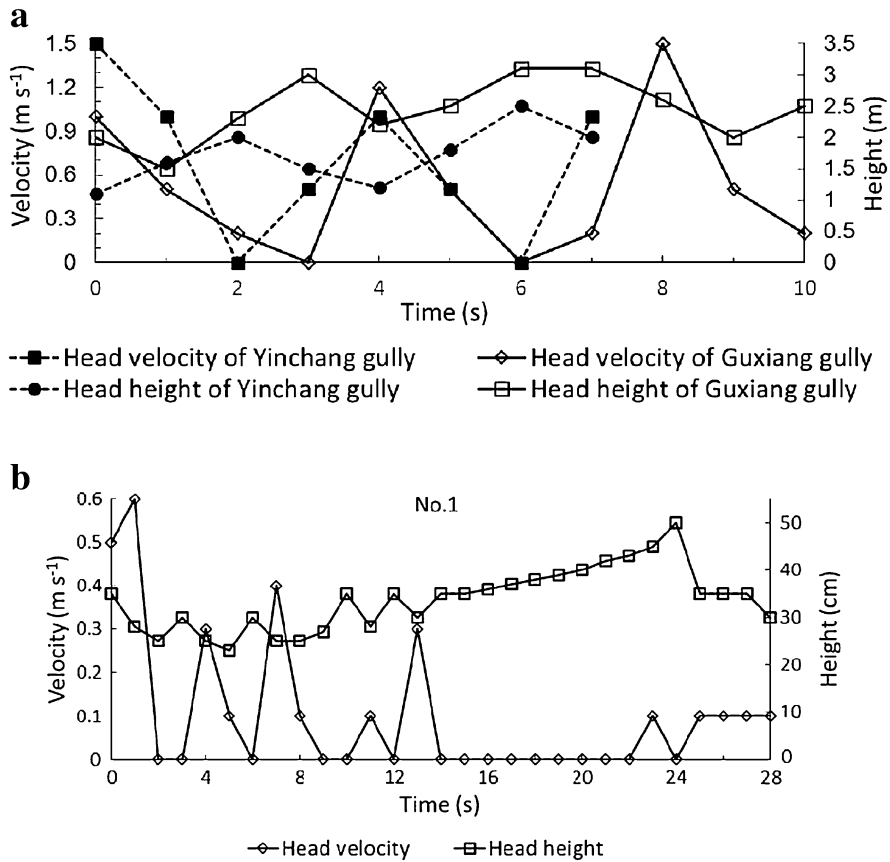


Fig. 6 Motions of field and experimental two-phase debris flows. **a** Motion of natural two-phase debris flows, **b** motion of an experimental two-phase debris flow

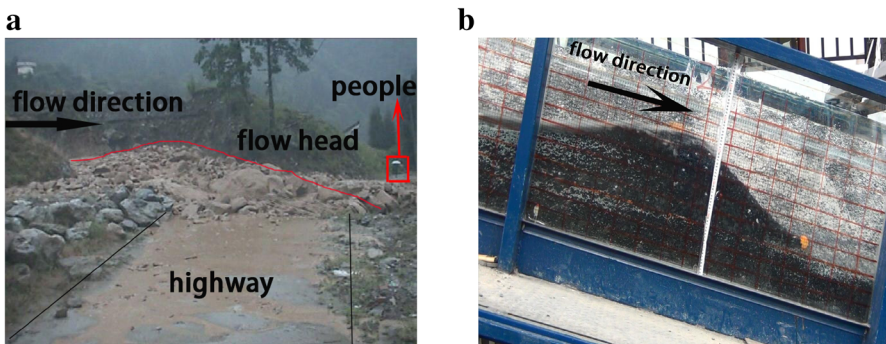


Fig. 7 Flow head of field and experimental two-phase debris flows. **a** Debris flow head in the Yinchang Gully, **b** debris flow head of experiment No. 1

stresses were assumed to satisfy the Mohr–Coulomb plasticity criterion, and as the normal pressure of the flow head continued to increase, the lateral pressure also increased. When the potential energy of the debris flow head became large enough to offset the energy consumption by the head friction, which incorporated the internal interaction of the media with itself and its interaction with the basal surface and the lateral surface, the flow head started to move again. As shown in Fig. 6b, the velocity of the flow head was zero during a period between 14 and 22 s and the height increased continuously. The flow head started moving again at 23 s when the height and pressure potential energy of the flow head were large enough. Both the motion process and the head shape of the natural and experimental two-phase debris flows were very similar.

Figure 8 shows the velocity of some single particle tracers. Figure 8a, b show the velocities of the particle tracers during the interim period ($u_m = 0$), compared with those during the moving period ($u_m > 0$) shown in Figs. 8c, d. Assuming that the position of the highest point of the flow head inside the flume was zero, both experiments No. 1 and 5 showed that the velocities of particles and water at locations 2–0.7 m behind the flow head were fairly stable, however, the velocities at locations within 0.7 m behind the head decreased rapidly. This observation indicated that the water and particles flow passed the kinetic energy to the debris flow head. The water content of the flow head was very low, and when the water flow reached the highest point of the head, it moved in the form of seepage. As a result, no water flow was observed on the surface at the front part of the flow head and the water content of the front was zero. Depending on whether the velocity of the debris flow head is zero, the flow process of the head is an alternation process of the interim period and the moving period. However, in each case the individual particles may stop before, at, or after the position $x = 0$ due to inertia. For example, particle 3 may

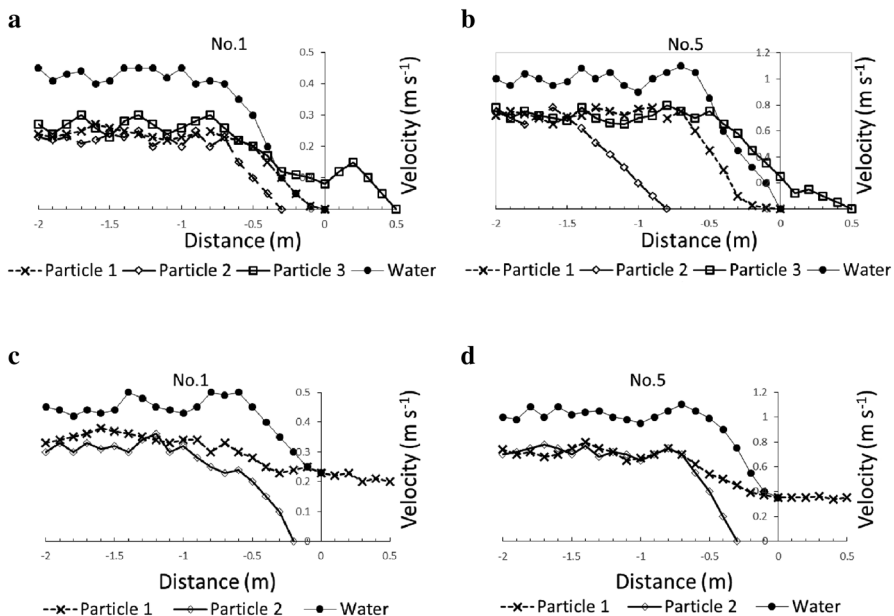


Fig. 8 Velocities of individual particles and average velocity of water flow. **a** ($u_m = 0$), **b** ($u_m = 0$), **c** ($u_m > 0$), **d** ($u_m > 0$)

initially accelerate due to the high gradient of the frontal surface and then decelerate due to friction (Fig. 8a).

4 Discussion

The power of the water flow released from the tank was converted into the kinetic energy of the particles flow and the water flow behind the debris flow head. Because the average velocity of the water flow was faster than the average velocity of the particles flow, which were both faster than the velocity of the debris flow head, the water and particles flow behind the debris flow head passed the kinetic energy to the flow head. Hence, the power of the water flow released from the tank was converted into the mechanical energy of the head and heat energy due to collisions and friction between particles. Simplifying the shape of the debris flow head as a triangular wedge, the height of the head H_m is the height of the triangle and the height of the center of gravity of the head is $H_m/3$. The assumption of a triangular flow head was made so that the pressure potential energy, E_p (with respect to the flume base datum) and the kinetic energy E_k per volume of the debris flow head at a given x -location along the flume axis can be determined by:

$$E_p = \frac{1}{3} \rho_m g H_m, \quad (1)$$

$$E_k = \frac{1}{2} \rho_m u_m^2, \quad (2)$$

Figure 9 shows the pressure potential energy, E_p , and the kinetic energy, E_k , of the debris flow head along the flume.

During the initial stage of the debris flow formation, the kinetic energy decreased and the pressure potential energy increased. During the process of intermittent motion, the pressure potential energy of the flow head increased with fluctuation, and the peak value of the pressure potential energy tended to be stable at locations 7 to 9.5 m of the flume. The fluctuation of the kinetic energy was more intense compared to that of the pressure potential energy. The lower the water flow discharge released from the tank, the more intense the fluctuation of the kinetic energy. The kinetic energy and pressure potential energy somehow transformed into each other during the process of intermittent motion. The decrease of the kinetic energy often was accompanied by the increase of the pressure potential energy. In the interim, the kinetic energy of the head was zero, but the pressure potential energy substantially increased. For a more complete and detailed study of the total energy of mass flows that include kinetic, pressure potential, gravity potential, and friction, and the energy conservation, refer to Pudasaini and Domnik [63].

Considering a unit width of the debris flow head moving down a flume. In the x direction, the kinetic energy per second provided by the particles flow and water flow behind the head are e_k^s and e_k^f , written as:

$$e_k^s = \frac{1}{2} \rho_s \overline{u_s^3} h, \quad (3)$$

$$e_k^f = \frac{1}{2} \rho_f \overline{u_f^3} h, \quad (4)$$

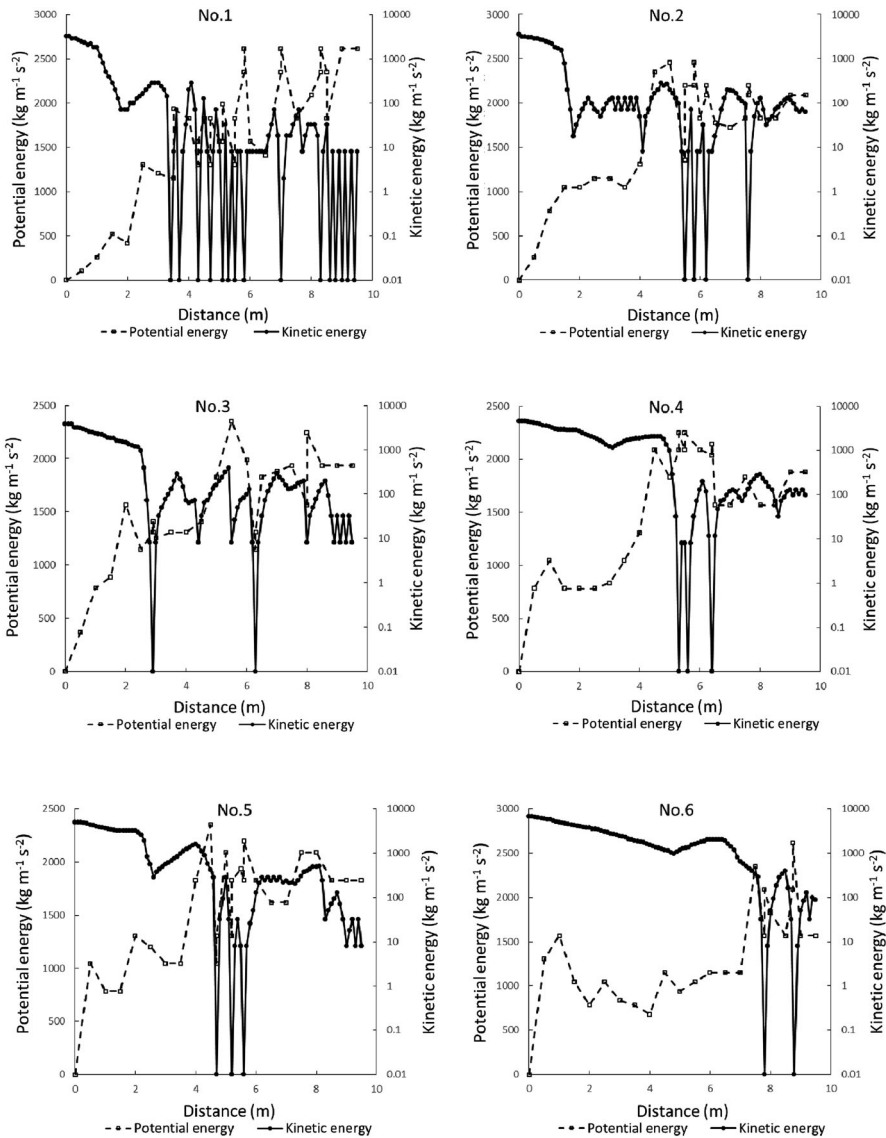


Fig. 9 Kinetic (E_k) and pressure (E_p) energy

The total kinetic energy per second resulting from the water flow and particles flow behind the debris flow head is e_k , written as:

$$e_k = e_k^s + e_k^f, \quad (5)$$

The energy per second provided by the debris flow head itself as it moves down the flume is p_m , written as:

$$p_m = \frac{1}{2} \rho_m g H_m l_m \overline{u_m} S, \quad (6)$$

In Eqs. (4), (5), and (6), the superscripts f , s , and m represent the liquid phase, the solid phase, and the mixture of solid phase and liquid phase, respectively. S is the gully slope, $S = \sin \theta$. Moreover, $\rho_s = c_g \rho_g$ and $\rho_f = c_w \rho_w$ are the densities of the solid and liquid phases, where c_g and c_w are the volume concentrations of the particles and water; ρ_g is the material density of the particles; and ρ_w is the density of the water. The variables \overline{u}_s and \overline{u}_f are the depth-averaged velocities of the solid and liquid phases behind the debris flow head. The parameters ρ_m and l_m are the density and length, and variable u_m , is the velocity of the debris flow head, where $\rho_m = c_g \rho_g + c_w \rho_w$. It is important to note that as c_g and c_w may vary substantially or, strongly in time and space, only the real two-phase mass flow model, such as that presented by Pudasaini [11], can provide the actual dynamic evolution of the mixture density ρ_m . The variables H_m and h are the height of the debris flow head and the height of the body flow layer behind the flow head. Because the height decreases from the head to the body, the length of the head is defined as the distance from the head front to the body section whose height is less than $0.2H_m$.

The power of the water flow released from the tank was partly consumed due to the turbulence in the water and collisions between the particles, and partly converted into the kinetic energy of the particles and the water flow behind the debris flow head. As shown in Fig. 5, during the initial stage of the debris flow motion, the depth-averaged velocity of the water and particles behind the head were fast and continued to decelerate. Then the depth-averaged velocity of the water flow and particles flow at the body became relatively stable during the process of intermittent motion of the flow head.

The following variables were defined: \overline{u}_s and \overline{u}_f represent the average value of the depth-averaged velocities of the solid phase and fluid phase which were stable relatively from 7 to 9.5 m of the flume; \overline{h} represents the average height of the body flow layer from 7 to 9.5 m of the flume.; and \overline{e}_k^s and \overline{e}_k^f represent the stable kinetic energy per second of the solid phase and liquid phase behind the debris flow from 7 to 9.5 m. The relations between these parameters can be expressed as:

$$\overline{e}_k^s = \frac{1}{2} \rho_s \overline{u}_s^3 \overline{h}, \quad (7)$$

$$\overline{e}_k^f = \frac{1}{2} \rho_f \overline{u}_f^3 \overline{h}, \quad (8)$$

$$\overline{e}_k = \overline{e}_k^s + \overline{e}_k^f, \quad (9)$$

The power of water flow released from the tank was $p_w = \gamma_w Q S$. As shown in Fig. 10, \overline{e}_k^s , \overline{e}_k^f and \overline{e}_k increased as the water flow power, p_w , increased. When the water flow power was lower, the ratio of the water flow power converting into the total kinetic energy of the particles and the water flow behind the flow head was lower, which indicated that the energy consumption ratio of the particles behind the flow head was high. On the contrary, when the water flow power was higher, the ratio of the water flow power converting into the total kinetic energy of the particles and the water was higher, which indicated that the energy consumption ratio of the particles behind the flow head was low. This phenomenon may be related to the frequency of collisions between the particles. Low water power means low water discharge and high sediment concentration behind the flow head as given in Table 1, which leads to a high frequency of particle collisions and a high energy consumption rate. Assuming that the ratio of the power of water flow released from the

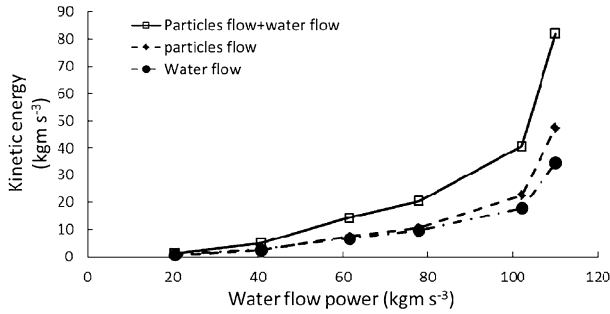


Fig. 10 Kinetic energy of water flow and particles flow behind the debris flow head

tank converting into the total kinetic energy of the particles and the water flow behind the flow head is k_1 , $0 < k_1 < 1$, hence,

$$e_k = k_1 p_w = k_1 \gamma_w Q S, \quad (10)$$

The power of the water flow released from the tank was partly converted into the kinetic energy of the particles and the water flow behind the debris flow head, then the total kinetic energy of the particles and the water flow behind the debris flow head was partly converted into the kinetic energy of the debris flow head, and partly consumed by coulomb friction of the debris flow head. By assuming coulomb friction of the debris flow head is a product of the weight of the particles and the dynamic friction coefficient k_2 , $0 < k_2 < 1$, this assumption incorporates the internal interaction of the media with itself and its interaction with the basal surface and the lateral surface. This simple expression can be used to get information about flow characteristics without requiring the full equations of motion or determining all the friction parameters from the experimental or field observations [63]. The consumed energy per second, e_d , by particles of the debris flow head is a product of the shear stress and velocity of the debris flow head, hence,

$$e_d = \frac{1}{2} k_2 \gamma_g c_g H_m l_m u_m, \quad (11)$$

The consumed energy is the sum of the total kinetic energy of the particles and the water flow behind the debris flow head and the energy, p_m , provided by the debris flow head itself. Hence,

$$e_d = e_k^s + e_k^f + p_m, \quad (12)$$

Incorporating Eqs. (5), (6), (10) and (11) into Eq. (12), one obtains:

$$\overline{u_m} = \frac{2k_1 S}{\left(k_2 c_g \frac{\gamma_g}{\gamma_w} - S \frac{\gamma_m}{\gamma_w}\right) H_m l_m} \frac{Q}{\gamma_w}, \quad (13)$$

Using Eq. (13) and the parameters and variables from the experiments, $\overline{u_m}$, H_m , l_m , S , γ_m , γ_w , and γ_g , the values of k_1 and k_2 were calculated using the least-squares method. The values of some of the parameters were: $S = 0.31$, $\gamma_w = 9.8 \times 10^3 \text{ kg/m}^3$, $\gamma_g = 2.6 \times 10^4 \text{ kg/m}^3$, and Q was the constant water flow discharge released from the tank listed in Table 1. The sediment volume content, c_g , and the water volume content, c_w , of

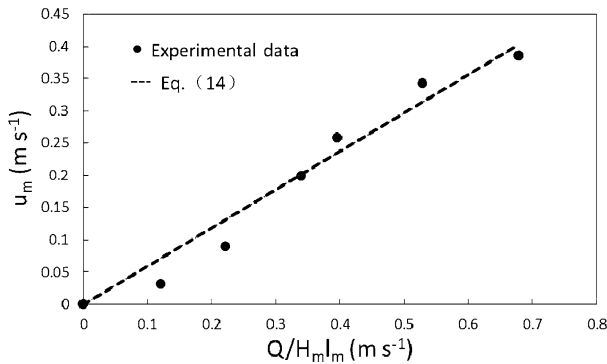


Fig. 11 Comparison between computed and observed values of u_m and $Q/H_m l_m$

the debris flow head were between 60 and 61.9 % and 1.2 and 3.2 %, respectively, as listed in Table 1, which varied little. The sediment volume content was assumed to be $c_g \approx 61$ % and the water volume content was $c_w \approx 2.2$ %, hence, the density of the head was $\rho_m = c_g \rho_g + c_w \rho_w \approx 1.64 \times 10^3 \text{ kg/m}^3$. Assuming $\bar{u}_m = \bar{u}_m = L/T$, where L and T are the length of the flume and the length of time that it took the debris flow head to move through the flume. $H_m = \bar{H}_m$, $l_m = \bar{l}_m$, where \bar{H}_m , \bar{l}_m were the average height and length of the debris flow head through the flume, which was assumed to be one half of the average height and length of the debris flow head at 7–9.5 m. The results were $k_1 = 0.46$ and $k_2 = 0.59$. And substituting k_1 , k_2 into Eq. (13), one obtains:

$$\bar{u}_m = \frac{0.92S}{\left(0.59c_g \frac{\gamma_g}{\gamma_w} - S \frac{\gamma_m}{\gamma_w}\right) H_m l_m} \frac{Q}{H_m l_m}, \quad (14)$$

As shown in Fig. 11, Eq. (14) is in good agreement with the experimental data. The velocity of the debris flow head was proportional to the flood discharge and inversely proportional to the height and length of the debris flow head. The conclusion that the velocity of the debris flow head was proportional to the flood discharge is in good agreement with other experiments [40, 54]. The flood discharge represented the supply of energy, while the height and length of the debris flow head represented energy consumption by the particles. The data and results presented here are important as these can be utilized to validate the two-phase debris flow mass models [11, 12] with strong solid fluid interactions.

5 Conclusions

The field surveys and flume experiments showed that the head motion of two-phase debris flows is intermittent. The height of the head of a debris flow increases gradually during the initiation stage and reaches equilibrium at a certain distance. The height growth and the velocity of the flow head show fluctuation characteristics. Because the average velocity of the water flow is faster than that of the particles flow, and both are faster than the velocity of the debris flow head, the water and particles flow behind the debris flow head pass their kinetic energy to the flow head. The energy consumption of the debris flow head is obvious

due to collisions between the particles. When the energy supply of the water flow and particles passing to the head is not enough to offset the energy consumption, the debris flow head stagnates and waits for more energy supply from the water and particles. Only when the energy of the flow head accumulates to a certain value then the flow head starts to move. With the increase of the flow water discharge, the energy supply of the water flow and the particles flow behind the head becomes larger and the number of interim periods becomes smaller. The energy supply of the water flow and particles flow and the energy consumption of the debris flow head determine the unsteady motion of two-phase debris flows. The analyses have proven that the average velocity of the two-phase debris flow head is proportional to the flood discharge and inversely proportional to the volume of the debris flow head.

Acknowledgments This study is supported by the Key Deployment Project of the Chinese Academy of Sciences (Grant No. KZZD-EW-05-01) and the National Natural Science Foundation of China (Grant No. 20141300833).

Open Access This article is distributed under the terms of the Creative Commons Attribution 4.0 International License (<http://creativecommons.org/licenses/by/4.0/>), which permits unrestricted use, distribution, and reproduction in any medium, provided you give appropriate credit to the original author(s) and the source, provide a link to the Creative Commons license, and indicate if changes were made.

References

1. Dowling CA, Santi PM (2014) Debris flows and their toll on human life: a global analysis of debris-flow fatalities from 1950 to 2011. *Nat Hazards* 71(1):203–227
2. Huang X, Tang C (2014) Formation and activation of catastrophic debris flows in Baishui River basin, Sichuan Province, China. *Landslides* 11(6):955–967
3. Iverson RM (1997) The physics of debris flows. *Rev Geophys* 35(3):245–296
4. Armanini A, Fraccarollo L, Rosatti G (2009) Two-dimensional simulation of debris flows in erodible channels. *Comput Geosci* 35(5):993–1006
5. Bagnold RA (1954) Experiments on a gravity-free dispersion of large solid spheres in a Newtonian fluid under shear. *Proc R Soc Lond A* 225(1160):49–63
6. Coussot P, Ancey C (1999) Rheophysical classification of concentrated suspensions and granular pastes. *Phys Rev E* 59(4):4445
7. Takahashi T (1978) Mechanical characteristics of debris flow. *J Hydraul Div ASCE* 104(8):1153–1169
8. Armanini A, Capart H, Fraccarollo L, Fraccarollo L, Larcher M (2005) Rheological stratification in experimental free-surface flows of granular–liquid mixtures. *J Fluid Mech* 532:269–319
9. Wang ZY, Lee JHW, Melching CS (2014) River dynamics and integrated river management. Springer Verlag/Tsinghua Press, Berlin/Beijing, pp 226–230
10. Wang ZY, Wai OWH, Cui P (1999) Field investigation on debris flows. *Int J Sedim Res* 14(4):10–23
11. Pudasaini SP (2012) A general two-phase debris flow model. *J Geophys Res* 117(F3):1–28
12. Pudasaini SP (2014) Dynamics of submarine debris flow and tsunamis. *Acta Mech* 225(8):2423–2434
13. Kafle J, Pokhrel PR, Khattri KB, Kattel P, Tuladhar BM, Pudasaini SP (2016) Landslide-generated tsunami and particle transport in mountain lakes and reservoirs. *Ann Glaciol* 57(71):232–244
14. Pudasaini SP, Krautblatter M (2014) A two-phase mechanical model for rock-ice avalanches. *J Geophys Res* 119(10):2272–2290
15. Kattel P, Khattri KB, Pokhrel PR, Kafle J, Tuladhar BM, Pudasaini SP (2016) Simulating glacial lake outburst floods with a two-phase mass flow model. *Ann Glaciol* 57(71):349–358
16. Coussot P (1997) Mudflow rheology and dynamics. Balkema, Rotterdam
17. Fraccarollo L, Papa M (2000) Numerical simulation of real debris-flow events. *Phys Chem Earth Part B* 25(9):757–763
18. Johnson AM, Rohm PH (1970) Mobilization of debris flows. *Z Geomorphol Supplementband* 9:168–186
19. Yano K, Daido A (1965) Fundamental study on mudflow. *Bull Disaster Prev Res Inst* 14(2):69–83
20. Julien PY, Lan Y (1991) Rheology of hyperconcentrations. *J Hydraul Eng* 117(3):346–353

21. Iverson RM, Denlinger RP (1987) The physics of debris flows—a conceptual assessment. In: Beschta RL (ed) *Erosion and sedimentation in the Pacific Rim*. IAHS Publication, Wallingford, pp 155–165
22. Wang ZY (2002) Free surface instability of non-Newtonian laminar flow. *J Hydraul Res* 40(4):449–460
23. Wang ZY, Larsen P, Nestmann F, Ditttrich A (1998) Resistance and drag reduction of hyperconcentrated flows over rough boundaries. *J Hydraul Eng* 1:1–9
24. Kang ZC (1996) *Debris flow hazards and their control in China*. Science Press of China, Beijing (in Chinese)
25. Kang ZC, Lee CF, Ma AN, Ruo JT (2004) *Debris flow studies in China*. Science Press of China, Beijing (in Chinese)
26. Wang ZY, Cui P, Yu B (2001) The mechanism of debris flow and drag reduction. *J Nat Disasters* 10(3):37–43 (in Chinese)
27. Scheidl C, Rickenmann D (2010) Empirical prediction of debris-flow mobility and deposition on fans. *Earth Surf Proc Land* 35(2):157–173
28. Pierson TC (1980) Erosion and deposition by debris flows at Mt Thomas, north Canterbury, New Zealand. *Earth Surf Process* 5(3):227–247
29. Coe JA, Kinner DA, Godt JW (2008) Initiation conditions for debris flows generated by runoff at Chalk Cliffs, central Colorado. *Geomorphology* 96(3):270–297
30. Bonnet-Staub I (1999) Définition d’une typologie des dépôts de laves torrentielles et identification de critères granulométriques et géotechniques concernant les zones sources. *Bull Eng Geol Environ* 57(4):359–367
31. Takahashi T (2007) *Debris flows: mechanics, predictions and counter measures*. Taylor and Francis/Balkema, London/Rotterdam
32. Bagnold RA (1956) The flow of cohesionless grains in fluids. *Philos Trans R Soc Lond A* 249(964):235–297
33. Takahashi T (1981) Debris flow. *Ann Rev Fluid Mech* 13:57–77
34. Savage SB, McKeown S (1983) Shear stress developed during rapid shear of dense concentrations of large spherical particles between concentric cylinders. *J Fluid Mech* 127:453–472
35. Pudasaini SP (2011) Some exact solutions for debris and avalanche flows. *Phys Fluids* 23(4):043301
36. Arattano M, Marchi L (2005) Measurements of debris flow velocity through cross-correlation of instrumentation data. *Nat Hazards Earth Syst Sci* 5(1):137–142
37. Berti M, Genevois R, LaHusen R, Simoni A, Tecca PR (2000) Debris flow monitoring in the Acquabona watershed on the Dolomites (Italian Alps). *Phys Chem Earth Part B* 25(9):707–715
38. Hürlimann M, Rickenmann D, Graf C (2003) Field and monitoring data of debris-flow events in the Swiss Alps. *Can Geotech J* 40(1):161–175
39. Marchi C, Jommi C (2002) Modeling the shear strength of unsaturated soils. *Unsaturated Soils: Proceedings of the Third International Conference, UNSAT2002*, vol. 2. Taylor & Francis US, Recife, Brazil, p 245
40. Stancanelli LM, Lanzoni S, Foti E (2015) Propagation and deposition of stony debris flows at channel confluences. *Water Resour Res* 51(7):5100–5116
41. Lanzoni S, Tubino M (1993) Rheometric experiments on mature debris flows. *Proceedings of the congress—international association for hydraulic research. Local organization organizing committee of the congress of the XXV congress*, vol. 3. 1993, p 47
42. Wang ZY, Zhang XY (1989) Experimental study of initiation and laws of motion of debris flow. *Acta Geogr Sin* 44(3):291–301
43. Chen H, Crosta GB, Lee CF (2006) Erosional effects on runout of fast landslides, debris flows and avalanches: a numerical investigation. *Geotechnique* 56(5):305–322
44. Rémaitre A (2006) *Morphologie et dynamique des laves torrentielles: Applications aux torrents des Terres Noires du bassin de Barcelonnette (Alpes du Sud)*. Ph.D. thesis, Strasbourg, France, p 68
45. Rickenmann D, Weber D, Stepanov B (2003) Erosion by debris flows in field and laboratory experiments. In: Rickenmann D, Chen C-I (eds) *Debris-flow hazards mitigation: mechanics, prediction, and assessment*. Millpress, Rotterdam, pp 883–894
46. Fraccarollo L, Capart H (2002) Riemann wave description of erosional dam-break flows. *J Fluid Mech* 461:183–228
47. Berger C, McArdell B W, Schlunegger F (2011) Direct measurement of channel erosion by debris flows, Illgraben, Switzerland. *J Geophys Res* 116(F1):1–2
48. Reid ME, Iverson RM, Logan M, LaHusen, RG, Godt, JW, Griswold, JP (2011) Entrainment of bed sediment by debris flows: results from large-scale experiments. In: R. Genevois (ed) *Debris-flow hazards mitigation, mechanics, prediction, and assessment*, Millpress, Rotterdam, pp 367–374
49. Kean JW, McCoy SW, Tucker GE, Staley DM, Coe JA (2013) Run-off generated debris flow: observations and modeling of surge initiation, magnitude, and frequency. *J Geophys Res* 118(4):2190–2270

50. Suwa H (1988) Focusing mechanism of large boulders to a debris-flow front. *Trans Jpn. Geomorphol Union* 9:151–178
51. Takahashi TA (2009) Review of Japanese debris flow research. *Eros Control Eng* 2:1
52. Iverson RM, Reid ME, Lahusen RG (1997) Debris-flow mobilization from landslides. *Annu Rev Earth Planet Sci* 25:85–138
53. Miyazawa N (1998) Flow behavior of head of stone debris flow on unsaturated erodible bed. In: Jayawadena AW, Lee JHW, Wang ZY (eds) *River sedimentation—theory and application*. Balkema A.A. Publishers, Rotterdam, pp 295–301
54. Wang ZY, Wang GQ, Liu C (2005) Viscous and two-phase debris flows in southern China's Yunnan plateau. *Water Int* 30(1):14–23
55. Iverson RM (1997) The physics of debris flow. *Rev Geophys* 35:245–296
56. Major JJ (1997) Depositional processes in large-scale debris-flow experiments. *J Geol* 105:345–366
57. Denlinger RP, Iverson RM (2001) Flow of variably fluidized granular masses across three-dimensional terrain. *J Geophys Res* 106(B1):553–566
58. Cui P, Chen XQ, Wang YY, Hu KH, Li Y (2005) Jiang-jia Ravine debris flows in south-western China. In: Jakob M, Hungr O (eds) *Debris-flow hazard and related phenomena*. Springer, Berlin, pp 565–594
59. Kang ZC, Cui P, Wei FQ, He SF (2006) Data collection of observation of debris flows in Jiangjia Ravine, Dongchuan Debris Flow Observation and Research Station (1961–1984). Science Press of China, Beijing (**in Chinese**)
60. Luna BQ, Remaître A, Van Asch TWJ, Malet JP, Van Westen CJ (2012) Analysis of debris flow behavior with a one dimensional run-out model incorporating entrainment. *Eng Geol* 128:63–75
61. Takahashi T (1982) Study on the deposition of debris flows (3): erosion of debris fan. *Annu DPRI* 25B-2:327–348 (**in Japanese**)
62. Takahashi T (1987) High velocity flow in steep erodible channels. *Proc. IAHR Congress, Lausanne*, pp 42–53
63. Pudasaini SP, Domnik B (2009) Energy considerations in accelerating rapid shear granular flows. *Nonlinear Process Geophys* 16(3):399–407